Comparison of Models on the Prediction of Binary Equilibrium Data of Activated Carbons

A. Ahmadpour, K. Wang, and D. D. Do
Adsorption Engineering Science Group, Dept. of Chemical Engineering, The University of Queensland, St. Lucia, QLD 4072, Australia

A pure-component equilibrium adsorption isotherm of methane, ethane, propane, and CO_2 at different temperatures and the binary adsorption data of methane with the other three species measured at 500 torr (66.7 kPa) and temperatures of 273 K and 303 K are presented and discussed. These measurements were carried out on three nutshell-derived KOH chemically activated carbon (AC) samples and one commercial activated carbon. The binary adsorption data of another commercial AC (Nuxit-al) from the literature are also used for comparison purposes. The single and binary experimental data were applied to six models: IAST, loading-dependent isosteric heat, micropore-size distribution (MPSD), energy distribution (ED), extended Langmuir, and extended Sips models. The models were found to describe the experimental data of the commercial ACs with a reasonably good accuracy, but only the model assuming isosteric heat as a function of loading could reasonably predict the data of KOH chemically activated carbons.

Introduction

Activated carbon has been found to be a good candidate for the storage of natural gas (NG). Although the low density of adsorbed gas in this material is still one of the drawbacks for storage purposes, there have been many research activities in recent years to find better ways of increasing the adsorption density by modifying the structure of the carbonaceous materials. NG consists of mainly methane (85–95%) with a minor amount of ethane, and higher-order hydrocarbons, nitrogen, carbon dioxide, and sulfur compounds. These heavily adsorbing compounds are considered impurities and affect the adsorption of methane quite strongly. Therefore, studying the impact of these components on methane storage is very important. Also, knowledge of the interaction and competition of different gases in adsorption processes is necessary for design purposes.

One of the problems in multicomponent adsorption investigation is the need for obtaining data over wide ranges of pressure, temperature, and composition conditions to understand the competitive adsorption behavior of mixtures. Because of the substantial amount of time involved in conducting the experiments, there is scant information in the literature on mixture equilibria. Therefore, it is desirable to use the single-component adsorption isotherm data, which is easier to obtain experimentally, and to correlate them to predict mixture adsorption equilibria.

A comprehensive investigation of the effect of preparation methods and structural parameters on the adsorption behavior of activated carbons was carried out by the authors (Ahmadpour and Do, 1995, 1996, 1997; Nguyen et al., 1995; Wang et al., 1997). It is the objective of this study to investigate multicomponent adsorption equilibria in a series of activated carbons with different pore structures obtained by activation of macadamia nutshell (MNS) using KOH. These samples, with a different degree of microporosity in the structure (Ahmadpour and Do, 1997), are used to measure competitive interactions in binary adsorption of methane with ethane, propane, and carbon dioxide. Adsorption studies were also conducted with the same mixtures on the commercial activated carbon, Ajax, for comparison purposes. Furthermore the binary equilibrium data for Nuxit-al-activated carbon from the literature are also used to provide comparisons with the data obtained for nutshell carbons in our laboratories. Subsequently, six models were used to predict the multicomponent adsorption equilibria by using the single-component isotherm information. The models used for correlating the data are (1)

Correspondence concerning this article should be addressed to D. D. Do. The binary adsorption data are available upon request.

ideal adsorption solution theory (IAST) of Myers and Prausnitz (1965); (2) isosteric heat as a function of loading (IHFL) proposed by Do and Do (1997); (3) micropore size distribution (MPSD); (4) energy distribution (ED); (5) extended Langmuir (EL); and (6) Sips equation.

Theory

Ideal adsorption solution theory

Myers and Prausnitz (1965) presented the IAST based on a sound thermodynamic framework. This model, which is widely used as a standard for multicomponent equilibria, has some attractive features. First of all, IAST does not require any mixture data, and secondly it is independent of the actual model of physical adsorption since it is an application of solution thermodynamics to the adsorption problem (O'Brien and Myers, 1985). Applying the IAST requires the calculation of an integral equation to obtain the reduced spreading pressure. Most of the isotherm equations commonly used for describing the single-component data cannot be solved analytically for the spreading pressure. Therefore, the algorithm for the solution of the IAST equation requires numerical integrations at each step of the iteration procedure, and this is generally slow. O'Brien and Myers (1984) introduced a new adsorption isotherm equation and a procedure that allows fast computation of multicomponent adsorption equilibria. This isotherm equation, obtained by a truncation of two terms of the series expansion of the adsorption integral equation in terms of the central moments of the adsorption energy distribution, has the following form:

$$\theta_i = \frac{\eta_i}{1+\eta_i} + \frac{\sigma_i^2 \eta_i (1-\eta_i)}{2(1+\eta_i)^3}, \tag{1}$$

where

$$\eta_i = b_i P_i. \tag{2}$$

The parameter σ_i^2 in Eq. 1 is the variance of the adsorption energy distribution for pure component i. The new algorithm, which is based on Eq. 1, is generally an order-of-magnitude faster than the IAST (O'Brien and Myers, 1985), and is called FASTIAS. The FASTIAS algorithm is used to predict the binary adsorption equilibria in this study.

Isosteric heat as a function of loading model

Recently, Do and Do (1997) proposed an isotherm equation based on the isosteric heat as a function of loading (IHFL). In their model the variation of isosteric heat with loading is regarded as the measure of the heterogeneity of the adsorbent. This general model has been tested with single-component adsorption isotherm data of many adsorbates on different samples of activated carbons and zeolites with very good success. The basis of this new isotherm is to fit the experimental data of different adsorbates at various temperatures simultaneously to extract the adsorbate and solid property parameters. The final form of the equation is

$$\frac{\theta}{(1-\theta^{t_k})^{1/t_k}} = \frac{\beta P}{\sqrt{M_k T}} \exp\left\{ \frac{E_k(0)[1-\alpha f(\theta;c)] + u_{k,k}\theta}{RT} \right\}, \tag{3}$$

where θ is the fractional loading, t is the parameter related to the fractal dimensions of the solid and adsorbate; β is a parameter characterizing the solid property, $E(0)$ is the isosteric heat at zero loading, α is the extent of energy heterogeneity, $f(\theta;c)$ is a function describing the pattern of heterogeneity, and u is the adsorbate–adsorbate interaction. In this study, Eq. 3 has been extended to the multicomponent system to predict the binary adsorption data. The general form of the extended equation for the component i is

$$\frac{\theta_i}{\left[1-\left(\sum_{k=1}^{N}\theta_k\right)^{t_i}\right]^{1/t_i}} = \frac{\beta P_i}{\sqrt{M_i T}} \times \exp\left\{ \frac{E_i(0)\left[1-\alpha f\left(\sum_{k=1}^{N}\theta_k;c\right)\right] + \sum_{k=1}^{N}(u_{i,k}\theta_k)}{RT} \right\}, \tag{4}$$

where

$$P_i = P_T y_i. \tag{5}$$

The cross adsorbate–adsorbate interaction energy is assumed to take the form:

$$u_{i,k} = \frac{u_{i,i} + u_{k,k}}{2}. \tag{6}$$

The mole fraction of the component i in the adsorbed phase is calculated from:

$$x_i = \frac{\theta_i}{\sum_{k=1}^{N}\theta_k}. \tag{7}$$

To reduce the number of parameters in the IHFL model, the following assumptions are made: (1) the adsorbate–adsorbate interaction is negligible compared to that of the adsorbate–adsorbent interaction and therefore the term u is set to zero; (2) the saturation capacity is independent of temperature; and (3) the saturation capacity, $C_{\mu s,i}$, is a function of the adsorbate. The number of parameters in the optimization is $3+3N$, where N is the number of adsorbates. It should be noted that in each optimization, the MN isotherm curves (where M is a number of temperatures) are optimized altogether. By assuming the form for the pattern of heterogeneity for the solid is

$$f(\theta;c) = \frac{c\theta}{1+(c-1)\theta}, \tag{8}$$

the following equations were obtained for the binary mixtures:

$$\theta_1 = \frac{\beta y_1 P_T}{\sqrt{M_1 T}}[1-\theta_T^{t_1}]^{1/t_1}\exp\left[\frac{E_1(0)-\dfrac{\alpha E_1(0) c\theta_T}{1+(c-1)\theta_T}}{RT}\right] \quad (9)$$

$$\theta_2 = \frac{\beta y_2 P_T}{\sqrt{M_2 T}}[1-\theta_T^{t_2}]^{1/t_2}\exp\left[\frac{E_2(0)-\dfrac{\alpha E_2(0) c\theta_T}{1+(c-1)\theta_T}}{RT}\right] \quad (10)$$

$$\theta_T = \theta_1 + \theta_2. \quad (11)$$

These three nonlinear equations were solved simultaneously to obtain the adsorbed phase concentrations.

Micropore size distribution model

This approach is based on the assumption that the surface heterogeneity of activated carbon is induced by the size distribution of the slit-shaped micropores (MPSD). The micropore size distribution (MPSD) is regarded as the intrinsic characteristic of activated carbon, and adsorbates with different molecular sizes have access to different ranges of this microporous network. If $\theta(r, P, T)$ represents the local isotherm and $f(r)$ the MPSD function, the overall adsorption equilibria of species i can be expressed as the integral of the local isotherm over the micropore size range appropriate to that species:

$$\langle\theta\rangle = \int_{r_1}^{r_2}\theta(r,P,T)f(r)\,dr, \quad (12)$$

where r_1 and r_2 are the lower and upper limits of the pore half-width accessible to the adsorbate, respectively. If $\theta(r, P, T)$ is represented by the Langmuir equation and $f(r)$ by the gamma distribution function, the overall isotherm (Eq. 12) will take the following form (Wang and Do, 1997):

$$C_\mu = \int_{r_{\min}}^{\infty} C_{\mu s}(T)\frac{Pb(r)}{1+Pb(r)}\frac{q^{\gamma+1}r^\gamma e^{-qr}}{\Gamma(\gamma+1)}dr, \quad (13)$$

where $r_{\min}$ is the minimum accessible half-width of the pore, in which the adsorbate molecule has zero interaction energy (Wang et al., 1997). The saturation capacity $C_{\mu s}(T)$ takes the temperature-dependent form as follows:

$$C_{\mu s} = C_{\mu s}^0\exp[\delta(T-T_0)], \quad (14)$$

and the local adsorption affinity $b(r)$ is expressed as:

$$b(r) = \frac{\beta}{\sqrt{MT}}\exp\left[\frac{E(r)}{RT}\right]. \quad (15)$$

The preexponential term (β) takes the same form as that in the IHFL model and $E(r)$ is the adsorbate–adsorbent interaction energy taken as the negative of the potential energy minimum inside the pore of half-width r. The form of potential energy in a slit-shaped micropore depends on our assumption about pore configuration. In the present study, the pore walls are assumed as the combination of many parallel lattices separated by a distance Δ, and the potential energy will take the form of 10-4-3 potential (Steele, 1974):

$$\varphi(r,z) = \frac{5}{3}\epsilon_{sk}^*\left\{\frac{2}{5}\left[\left(\frac{\sigma_{sk}}{r+z}\right)^{10}+\left(\frac{\sigma_{sk}}{r-z}\right)^{10}\right] - \left[\left(\frac{\sigma_{sk}}{r+z}\right)^{4}+\left(\frac{\sigma_{sk}}{r-z}\right)^{4}\right] - \left[\left(\frac{\sigma_{sk}^4}{3\Delta(0.61\Delta+r+z)^3}\right)-\left(\frac{\sigma_{sk}^4}{3\Delta(0.61\Delta+r-z)^3}\right)\right]\right\}, \quad (16)$$

where

$$\epsilon_{sk}^* = \frac{6}{5}\pi\rho_s\epsilon_{sk}\sigma_{sk}^2\Delta, \quad (17)$$

σ_{sk} is the collision diameter between the carbon and the adsorbate molecules, and ρ_s is the number density of carbon centers per unit volume. The parameter ϵ_{sk}^* is the minimum interaction energy between an adsorbate molecule and the single lattice layer. The values of Δ and ρ_s are generally taken as 0.335 (nm) and 114 (nm^{-3}), respectively (Steele, 1974). Solving Eq. 16 for the minimum, the interaction energy as a function of pore size can be obtained.

Equation 13 is the general isotherm equation applicable to all species. By optimizing the model predictions with respect to the multiple-temperature isotherm data of many species simultaneously, the parameters characterizing the carbon structure (q, γ, β), and the isotherm parameters ($C_{\mu s}^0$, ϵ_{sk}^*, δ) can be extracted. With the optimized parameters, the multicomponent adsorption equilibria can then be predicted from the following equation:

$$C_{\mu,i} = \int_{r_{\min}}^{\infty} C_{\mu s,i}(T)\frac{P_i b_i(r)}{1+\sum_{k=1}^{N}P_k b_k(r)}\frac{q^{\gamma+1}r^\gamma e^{-qr}}{\Gamma(\gamma+1)}dr \quad (18)$$

$$b_i(r) = \frac{\beta}{\sqrt{M_i T}}\exp\left[\frac{E_i(r)}{RT}\right]. \quad (19)$$

It should be noted that Eq. 18 incorporates two distinguishing features: (1) the equilibrium interaction between different adsorbates is confined within the same pore where they are accommodated, and (2) the effect of size exclusion is accounted for; that is adsorbates compete with each other only in pores accessible to them.

Energy distribution model

The overall adsorption isotherm on a heterogeneous surface can also be expressed in terms of adsorption energy distribution (ED) as

$$\langle\theta\rangle = \int_{E_{\min}}^{E_{\max}} \theta(E,P,T)F(E)\,dE, \tag{20}$$

where $F(E)$ is the energy distribution function, $E_{\min}$ and $E_{\max}$ are the lower and upper limits for the energy distribution, respectively. The ED is related to MPSD by the expression

$$F(E)\,dE = f(r)\,dr. \tag{21}$$

Therefore, by knowing $f(r)$ for MPSD, the related energy distribution $F(E)$ can be derived by using Eq. 21. The multicomponent adsorption equilibria can then be written in terms of ED as

$$C_{\mu,i} = \int_{E_{\min,i}}^{E_{\max,i}} C_{\mu s,i}(T)\frac{P_i b_i(E_i)}{1+\sum_{k=1}^{N} P_k b_k(E_k)} F_i(E_i)\,dE_i. \tag{22}$$

In Eq. 22 the energy matching between different species takes the traditional cumulative energy-matching mechanism (Valenzuela et al., 1988):

$$\frac{E_i - E_{\min,i}}{E_{\max,i} - E_{\min,i}} = \frac{E_j - E_{\min,j}}{E_{\max,j} - E_{\min,j}}. \tag{23}$$

It should be pointed out that for the single-component system Eq. 22 is equivalent to Eq. 18; however, for the binary system the results may be different. The reason is that Eq. 22 assumes the uniform energy matching between different adsorbates, which is different from the "adsorbate–pore interaction" mechanism assumed in Eq. 18.

Extended Langmuir model

The Langmuir adsorption isotherm can be easily extended to the multicomponent adsorption system by keeping all the assumptions made by this model in the treatment of pure-component adsorption equilibria. In extending this model to multicomponent systems the amount adsorbed by the component i can be written as:

$$C_{\mu,i} = C_{\mu s}\frac{b_i P_i}{1+\sum_{k=1}^{N} b_k P_k}. \tag{24}$$

For the extended Langmuir (EL) model to be thermodynamically correct it is required that the saturation capacities of all components be the same. However, for physical adsorption of molecules of widely different sizes this assumption is unrealistic (Ruthven, 1984).

Sips model

In 1948, Sips proposed an empirical equation for the adsorption of pure component that is the combination of the Langmuir and Freundlich equations. This three-parameter equation has been widely used for fitting the isotherm data of different hydrocarbons on activated carbon. The Sips adsorption isotherm equation for pure component has the following form:

$$C_{\mu} = C_{\mu s}\frac{(bP)^{1/n}}{1+(bP)^{1/n}}. \tag{25}$$

Using the same analogy used for extending the single-component Langmuir equation to that for multicomponent adsorption, the following equation is obtained for the Sips model:

$$C_{\mu,i} = C_{\mu s}\frac{(b_i P_i)^{1/n}}{1+\sum_{k=1}^{N}(b_k P_k)^{1/n}}. \tag{26}$$

However, this equation only corresponds to a special case of surface energetic heterogeneity. For normal activated carbon in which the energy sites are highly correlated, the IAS theory should be used. Applying the IAST with the concept of hypothetical pure-component pressure results in the following equation (Rudzinski et al., 1995):

$$C_{\mu,i} = C_{\mu s}\frac{b_i P_i\left(\sum_{k=1}^{N} b_k P_k\right)^{1/n-1}}{1+\left(\sum_{k=1}^{N} b_k P_k\right)^{1/n}}. \tag{27}$$

It can be seen that Eq. 27, which is the correct form of the Sips multicomponent model, is different from Eq. 26. Equation 27 was used to predict the binary adsorption equilibrium of all the systems studied in the present investigation.

Experimental

The measurements of single and binary adsorption isotherms were conducted using the volumetric technique. A highly accurate and flexible system capable of measuring both the single and multicomponent isotherms of vapors and gases was designed using the VCR components. The system is presented in Figure 1. Binary experiments were performed at a constant pressure of 66.7 kPa and a temperature of 303 K for the following mixtures: CH_4–C_2H_6, CH_4–C_3H_8, and CH_4–CO_2. An experiment for the binary system of CH_4–CO_2 on one of the commercial activated carbons was also conducted at the same pressure, but at a temperature of 273 K. All the gases used in the experiments were supplied by BOC Gases Co., and had the following specifications: CH_4, C_2H_6, and C_3H_8 with CP grade ($>99\%$) and CO_2 with anaerobic grade ($>99.95\%$). These gases were used without any further treatment. The behavior of the binary mixtures was investigated in four different structured activated carbons. These adsorbents included the commercial activated carbon, Ajax, and three ACs derived from the activation of macadamia nutshell with a 25, 100 and 500 wt. % KOH to nutshell ratio, respectively. The experimental binary adsorption data for Nuxit-al AC was taken from the literature (Valenzuela and Myers, 1989) for comparison. The character-

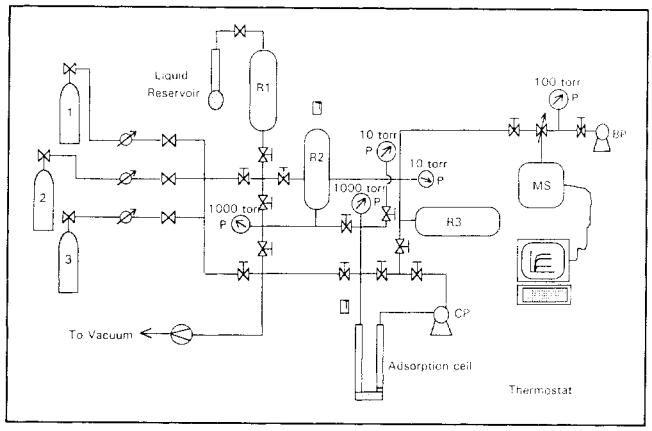

Figure 1. Multicomponent volumetric adsorption rig.

istics of Ajax-activated carbon are available in Do and Do (1997), and the preparation technique and physical properties of the nutshell-derived activated carbons are detailed elsewhere (Ahmadpour and Do, 1997). The following nomenclature is used to describe the nutshell carbon samples: NSK25, NSK100, and NSK500. In binary experiments, two-component gases were mixed in the R2 reservoir (with a volume of 1,218 cm^3) for a sufficient time to ensure good mixing, and then it was injected into the analysis section of the rig. The pressure in the analysis section was kept constant by adding small quantities of the mixture when the pressure decreased due to adsorption. The pressure in both dosing and analysis sections of the rig were measured with high accuracy Baratron-type (MKS) pressure transducers (P). The gas mixture was circulated through a precleaned activated-carbon sample bed in the adsorption cell by using a metal diaphragm bellows-pump (CP) -type MB-41E (Parker Hannifin Corp., USA). Circulation was continued for 7 h to ensure that true equilibrium was achieved. The gas in the analysis section was left for about one hour without circulation. A small volume of the gas phase, which is enclosed in the space among the three valves in the circulating line, was then directed to reservoir R3 (of volume 1980 cm^3) and diluted up to 10 times with helium. This mixture was finally sent to the mass spectrometer (MS) for quantitative analysis and the amount adsorbed was calculated from the mass balance.

Results and Discussion

Single-component adsorption

Adsorption isotherms of methane, ethane, propane, and carbon dioxide at different temperatures have been optimized simultaneously using IHFL and MPSD models. This was performed on the five different activated carbons mentioned in the previous sections. The optimization routine in the MATLAB software was used to minimize the sum square of residual between the experimental data and the model equations and then to extract the optimal parameters.

Table 1. Multicomponent Adsorption Models with the Number of Fitted Isotherms and the Number of Extracted Parameters

Model	No. of Isotherms	No. of Parameters
IAST	1	3
IHFL	14	15
MPSD	14	12
ED	14	12
EL	2	3
Sips	2	4

Table 2. Optimal Parameters and Average Relative Errors from Fitting the IHFL Model to Methane, Ethane, Propane, and CO_2 on Ajax-Activated Carbon

Component	Methane	Ethane	Propane	CO_2
$C_{\mu s}$ (mmol/g)	6.320	11.18	6.916	8.866
E (J/mol)	17,866	24,810	33,748	20,554
t	0.999	0.589	0.592	1.183
c	1.58			
α	0.237			
β	2.1×10^{-4}			
ARE (%)	5.0	6.5	7.9	6.0

Table 1 shows the number of single-component adsorption isotherms used in the optimization and the number of extracted parameters from each model. The reader should be aware that although the number of parameters in the IHFL, MPSD, and ED models are high, the isotherm data of many adsorbates at different temperatures are also used to obtain those parameters. Therefore, these models can be compared in terms of their predictions for multicomponent adsorption equilibria. The results of the optimizations are presented in Tables 2 to 6 for IHFL model and in Tables 7 to 11 for MPSD model. It should be mentioned that for Nuxit-al carbon the isotherm data of n-butane are also included in the optimization using the IHFL model. The comparison of fit of data by the models is based on the average relative error (ARE), which is listed in the tables for different adsorbates. The ARE is defined as (Kapoor and Yang, 1989):

$$\mathrm{ARE} = \frac{100}{N}\sum_{k=1}^{N}\mathrm{abs}\left(\frac{C_{\mu,\mathrm{cal}} - C_{\mu,\mathrm{exp}}}{C_{\mu,\mathrm{exp}}}\right)_k, \qquad (28)$$

where N is the number of data points, and $C_{\mu,\mathrm{cal}}$ and $C_{\mu,\mathrm{exp}}$ are the calculated and experimental amounts adsorbed, respectively.

It is apparent from analyzing results for different carbons using the IHFL model (Tables 2 to 6) that the adsorption capacities of NSK carbons for all species are higher than those of commercial activated carbons. In general the order of these carbons in terms of adsorption capacity is NSK500 > NSK100

Table 3. Optimal Parameters and Average Relative Errors from Fitting the IHFL Model to Methane, Ethane, Propane, n-Butane, and CO_2 on Nuxit-al-Activated Carbon

Component	Methane	Ethane	Propane	n-Butane	CO_2
$C_{\mu s}$ (mmol/g)	4.351	6.414	5.479	4.213	8.980
E (J/mol)	19,598	27,198	35,536	41,071	21,919
t	1.214	0.739	0.577	0.626	1.047
c	3.229				
α	0.131				
β	7.2×10^{-5}				
ARE (%)	2.6	1.8	2.2	6.1	4.1

Table 4. Optimal Parameters and Average Relative Errors from Fitting the IHFL Model to Methane, Ethane, Propane, and CO_2 on NSK25-Activated Carbon

Component	Methane	Ethane	Propane	CO_2
$C_{\mu s}$ (mmol/g)	7.265	8.375	4.242	8.058
E (J/mol)	18,346	30,924	40,491	20,682
t	0.427	0.288	0.349	0.673
c	0.287			
α	0.180			
β	6.0×10^{-4}			
ARE (%)	4.1	8.4	6.5	4.2

Table 5. Optimal Parameters and Average Relative Errors from Fitting the IHFL Model to Methane, Ethane, Propane, and CO_2 on NSK100-Activated Carbon

Component	Methane	Ethane	Propane	CO_2
$C_{\mu s}$ (mmol/g)	6.880	11.83	6.039	30.01
E (J/mol)	16,841	25,738	36,001	16,000
t	0.992	0.389	0.457	0.706
c	2.27			
α	0.101			
β	4.3×10^{-4}			
ARE (%)	17.3	5.1	9.0	8.0

Table 6. Optimal Parameters and Average Relative Errors from Fitting the IHFL Model to Methane, Ethane, Propane, and CO_2 on NSK500-Activated Carbon

Component	Methane	Ethane	Propane	CO_2
$C_{\mu s}$ (mmol/g)	8.801	22.27	11.53	26.79
E (J/mol)	18,437	27,455	38,449	19,058
t	1.081	0.350	0.329	3.232
c	1.71			
α	0.049			
β	1.0×10^{-4}			
ARE (%)	10.2	2.3	3.8	10.3

Table 7. Optimal Parameters and Average Relative Errors from Fitting the MPSD Model to Methane, Ethane, Propane, and CO_2 on Ajax-Activated Carbon

Component	Methane	Ethane	Propane	CO_2
$C_{\mu s}$ (mmol/g)	7.577	7.999	6.020	15.67
ϵ^*_{sk} (J/mol)	10,636	14,624	16,896	13,093
q	19.73			
γ	89.27			
β	8.9×10^{-5}			
δ	7.8×10^{-6}			
ARE (%)	4.5	1.9	1.6	2.2

Table 8. Optimal Parameters and Average Relative Errors from Fitting the MPSD Model to Methane, Ethane, Propane, and CO_2 on Nuxit-al-Activated Carbon

Component	Methane	Ethane	Propane	CO_2
$C_{\mu s}$ (mmol/g)	5.796	6.225	5.148	9.343
ϵ^*_{sk} (J/mol)	11,552	15,519	17,365	15,200
q	21.78			
γ	97.7			
β	3.5×10^{-5}			
δ	4.0×10^{-5}			
ARE (%)	3.5	1.7	3.2	3.4

Table 9. Optimal Parameters and Average Relative Errors from Fitting the MPSD Model to Methane, Ethane, Propane, and CO_2 on NSK25-Activated Carbon

Component	Methane	Ethane	Propane	CO_2
$C_{\mu s}$ (mmol/g)	6.066	4.417	3.312	10.62
ϵ^*_{sk} (J/mol)	11,267	16,389	18,985	14,568
q	36.59			
γ	155			
β	7.8×10^{-5}			
δ	4.8×10^{-5}			
ARE (%)	4.2	4.4	7.0	7.2

Table 10. Optimal Parameters and Average Relative Errors from Fitting the MPSD Model to Methane, Ethane, Propane, and CO_2 on NSK100-Activated Carbon

Component	Methane	Ethane	Propane	CO_2
$C_{\mu s}$ (mmol/g)	7.555	5.915	5.003	51.15
ϵ^*_{sk} (J/mol)	11,308	15,770	18,311	11,517
q	40.55			
γ	182.5			
β	1.4×10^{-4}			
δ	1.4×10^{-5}			
ARE (%)	10.0	3.4	9.6	25.9

Table 11. Optimal Parameters and Average Relative Errors from Fitting the MPSD Model to Methane, Ethane, Propane, and CO_2 on NSK500-Activated Carbon

Component	Methane	Ethane	Propane	CO_2
$C_{\mu s}$ (mmol/g)	5.735	10.087	8.072	51.74
ϵ^*_{sk} (J/mol)	10,160	17,544	19,708	14,213
q	39.44			
γ	180.6			
β	2.9×10^{-5}			
δ	1.6×10^{-4}			
ARE (%)	9.1	4.1	5.3	14.3

> NSK25 ≈ Ajax > Nuxit-al. In terms of energy of adsorption, the interaction between the adsorbate and adsorbent is increased with the increase in carbon number in the hydrocarbons. These values are also higher for CO_2 compared to methane because of the effect of the dipole moments of the carbon dioxide molecules. The parameter t, presented in the tables, reflects the heterogeneity of the carbon, and its value equal to unity implies a homogeneous surface. It is seen that there is no particular trend in the behavior of t, but in most cases it deviates from the ideal conditions ($t = 1$) for all species except methane.

The pattern of the heterogeneity parameter c in the IHFL model was found to be very low for NSK25 carbon, which means that there is a slow decay in the energy at low loading and a rapid decay when the loading approaches the monolayer coverage ($\theta = 1$). For the rest of the carbons, the values of c are between 1.6 and 2.9, indicating a sharp decay in the energy patterns at low coverage. The extent of heterogeneity

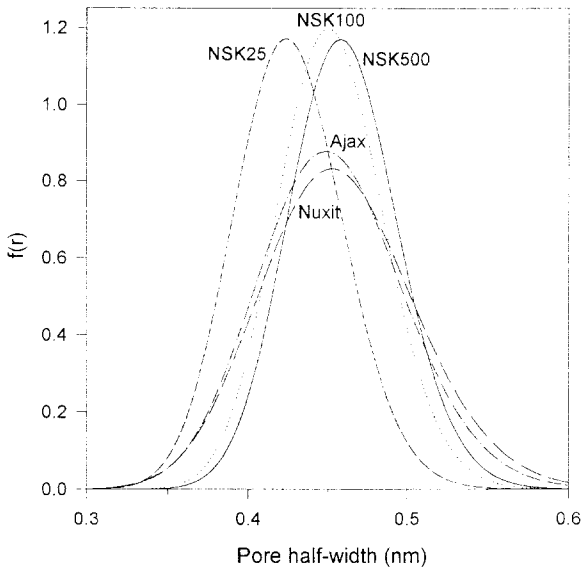

Figure 2. Pore-size distribution of activated carbons obtained from MPSD model.

α is found to decrease with an increase in the chemical-to-nutshell ratio in the series of NSK carbons, indicating that the NSK carbon becomes more homogeneous when the ratio of chemical to nutshell increases. The values of β, which is the adsorption affinity at infinite temperature and independent of the adsorbates, are in the same order for all carbons studied here, and these values are similar to the previous finding by Do and Do (1997).

The optimal parameters obtained by applying the MPSD model to activated carbons (Tables 7 to 11) show that for methane the saturation concentration is very close to the values obtained from the IHFL model, but for ethane and propane these values are generally lower. The differences are due to the sensitivity of the MPSD model to the pore and the adsorbate sizes. In terms of the interaction energies, a trend similar to that found in the IHFL model can be seen.

Examination of the tables for relative errors indicated that most of the errors are less than 10%, except for some high deviation for the NSK100 and NSK500 carbons. The fit seems to be very good for all species in Ajax- and Nuxit-al-activated carbons. The difference in the goodness of fit between the two sets of carbons, the commercial ACs, and the NSK series, seems to be from differences in the activation processes used in the preparation of these adsorbents. Usually, most commercial activated carbons are produced by physical activation, and have a small number of functional groups and other imperfections in their structure. On the other hand,

Table 13. Optimal Parameters and Average Relative Errors from Fitting the Sips and Extended Langmuir Models to the Single-Component Data of Methane–Ethane, Methane–Propane, and Methane–CO_2 on Nuxit-al-Activated Carbon at 293 K

	Sips	Extended Langmuir
	CH_4, C_2H_6	CH_4, C_2H_6
$C_{\mu s}$ (mmol/g)	5.62	3.93
n	1.44	—
b_1	7.2×10^{-4}	2.7×10^{-3}
b_2	1.5×10^{-2}	4.1×10^{-2}
ARE (%)	5.3, 2.7	11.7, 5.8

NSK carbons have been produced by the chemical-activation technique, which produces a considerable number of functional groups on the carbon surface compared to the physically activated carbons (Otowa et al., 1996). The effect of these functional groups on the adsorption behavior of activated carbons have not been fully investigated. The deviation of some of the models from the experimental data is thought to be due to the effect of these surface functional groups on the adsorption.

The adsorption affinity β for NSK100 is seen to be one order of magnitude higher than that for NSK500, indicating the narrower pore size distribution in NSK100 compared to NSK500. Very low values of δ for all carbons indicate that the adsorption capacity is independent of temperature over the temperature range studied.

Figure 2 shows PSD plots obtained from the MPSD model for all the activated carbons studied. It is clear from the figure that the mean pore size is shifted to higher values for the carbons in the NSK series, and also the distribution of pores is narrower for these carbons than for the commercial ACs. The reason is the different activation processes. The physical activation technique usually creates larger pores than does the KOH activation technique (Ahmadpour and Do, 1996). The higher adsorption energies of NSK carbons compared to the commercial ones, which can be seen from the result of both IHFL and MPSD models, come from the smaller mean pore size as well as the narrower PSD of the chemically activated carbons.

In studying the effect of the Sips model, the adsorption capacity and the parameter n were considered to be equal for the different species. Parameter n in the Sips equation shows the heterogeneity of the system, and its value is usually greater than unity. Therefore, the larger the n value, the more heterogeneous is the system. Tables 12 to 16 show the optimal parameters and relative errors of the Sips model as well as the EL model for different sets of adsorbates in all the

Table 12. Optimal Parameters and Average Relative Errors from Fitting the Sips and Extended Langmuir Models to the Single-Component Data of Methane–Ethane, Methane–Propane, and Methane–CO_2 on Ajax-Activated Carbon at 303 K

	Sips			Extended Langmuir		
	CH_4, C_2H_6	CH_4, C_3H_8	CH_4, CO_2	CH_4, C_2H_6	CH_4, C_3H_8	CH_4, CO_2
$C_{\mu s}$ (mmol/g)	7.49	6.48	11.3	4.16	4.35	4.74
n	1.53	1.93	1.18	—	—	—
b_1	4.7×10^{-4}	2.0×10^{-4}	7.2×10^{-4}	3.7×10^{-3}	3.5×10^{-3}	3.2×10^{-3}
b_2	1.0×10^{-2}	6.4×10^{-2}	2.0×10^{-3}	5.0×10^{-2}	0.26	8.8×10^{-3}
ARE (%)	3.1, 18.4	5.3, 10.6	6.4, 8.9	11.7, 21.8	11.5, 21.6	11.0, 21.8

Table 14. Optimal Parameters and Average Relative Errors from Fitting the Sips and Extended Langmuir Models to the Single-Component Data of Methane–Ethane, Methane–Propane, and Methane–CO_2 on NSK25-Activated Carbon at 303 K

	Sips			Extended Langmuir		
	CH_4, C_2H_6	CH_4, C_3H_8	CH_4, CO_2	CH_4, C_2H_6	CH_4, C_3H_8	CH_4, CO_2
$C_{\mu s}$ (mmol/g)	3.81	3.21	7.49	3.36	2.88	4.72
n	1.32	1.65	1.24	—	—	—
b_1	5.4×10^{-3}	4.6×10^{-3}	2.1×10^{-4}	9.6×10^{-3}	1.2×10^{-2}	6.1×10^{-3}
b_2	0.14	2.36	8.2×10^{-3}	0.20	3.47	2.2×10^{-2}
ARE (%)	3.3, 11.3	2.6, 13.7	3.9, 5.4	2.5, 13.0	2.5, 13.5	3.2, 6.8

activated carbons investigated in the present study. It is seen from the tables that the adsorption capacities are increased for almost all sets of adsorbates in the NSK carbon series. Adsorption affinity values are seen to be changed within four orders of magnitudes, and they do not follow any particular trend. The ARE values again show that the errors are higher for NSK carbons with the high chemical ratio.

Binary adsorption

The binary interaction of methane with other heavier hydrocarbons and CO_2 was studied on the different-structured activated carbons in order to get some insight into the real behavior of the storage of methane in the presence of other species. Figure 3 shows the experimental data (symbols) for adsorption on Ajax activated carbon for the three binary systems, along with the predictions from various models (lines). In all the binary adsorption graphs, the amounts adsorbed by the two species are plotted vs. the mole fraction of methane in the gas phase. A temperature of 303 K was chosen for all experiments, as it is the case in practical usage. It is seen from the figure that for the methane–CO_2 system the adsorption amount increases or decreases linearly with the methane mole fraction. This behavior is expected, as the interaction of both species with the carbon surface is almost the same. Within experimental error, the model's predictions are generally good for this system. For the other two binary systems, as the hydrocarbon molecules become larger, the adsorption interaction becomes higher. For methane–ethane system only the IAST model overpredicts the ethane adsorption, while other models are in good agreement with the experimental data. A similar result can be seen for the methane–propane case, the only difference being that the Sips model slightly underpredicts the amount of methane adsorption. The differences between the model predictions and the experimental data seem to originate from how well the pure-component data fit. It is known that a small error in fitting the single-component equilibrium data can cause a large error in the multicomponent prediction. To see the effect of temperature on adsorption behavior in the binary system, the binary adsorption data of methane and CO_2 on Ajax-activated carbon at 273 K and 66.7 kPa are presented in Figure 4. The same behavior can be observed at lower temperature, except the amount adsorbed is larger. The model's predictions are also similar to those at higher temperature. The binary adsorption equilibria of methane and ethane at 293 K on Nuxit-al-activated carbon are shown in Figure 5. For this carbon all of the models predict the experimental data very well.

The adsorption behavior of binary systems on NSK25 carbon is presented in Figure 6. For the case of methane and CO_2, only the MPSD model can predict the data of both species. The other models underpredict methane adsorption with different degrees of deviation. Underprediction of the amount of methane adsorbed by all models is seen for the other two binary systems as well. In the methane–ethane sys-

Table 15. Optimal Parameters and Average Relative Errors from Fitting the Sips and Extended Langmuir Models to the Single-Component Data of Methane–Ethane, Methane–Propane, and Methane–CO_2 on NSK100-Activated Carbon at 303 K

	Sips			Extended Langmuir		
	CH_4, C_2H_6	CH_4, C_3H_8	CH_4, CO_2	CH_4, C_2H_6	CH_4, C_3H_8	CH_4, CO_2
$C_{\mu s}$ (mmol/g)	9.12	5.42	15.46	4.99	4.42	7.06
n	1.55	1.86	1.20	—	—	—
b_1	5.0×10^{-4}	6.0×10^{-4}	6.2×10^{-4}	4.0×10^{-3}	4.7×10^{-3}	2.7×10^{-3}
b_2	1.0×10^{-2}	0.46	2.6×10^{-3}	5.1×10^{-2}	1.02	1.0×10^{-2}
ARE (%)	23.4, 20.0	12.9, 17.1	14.7, 4.9	12.9, 19.5	13.8, 16.6	13.3, 6.2

Table 16. Optimal Parameters and Average Relative Errors from Fitting the Sips and Extended Langmuir Models to the Single-Component Data of Methane–Ethane, Methane–Propane, and Methane–CO_2 on NSK500-Activated Carbon at 303 K

	Sips			Extended Langmuir		
	CH_4, C_2H_6	CH_4, C_3H_8	CH_4, CO_2	CH_4, C_2H_6	CH_4, C_3H_8	CH_4, CO_2
$C_{\mu s}$ (mmol/g)	10.37	7.39	11.77	6.83	6.28	10.84
n	1.39	1.54	1.02	—	—	—
b_1	6.1×10^{-4}	6.9×10^{-4}	1.4×10^{-3}	2.7×10^{-3}	3.0×10^{-3}	1.6×10^{-3}
b_2	1.5×10^{-2}	0.26	5.3×10^{-3}	4.4×10^{-2}	0.43	6.0×10^{-3}
ARE (%)	9.6, 22.3	3.7, 21.1	8.5, 5.4	13.9, 17.0	13.5, 18.1	11.9, 3.3

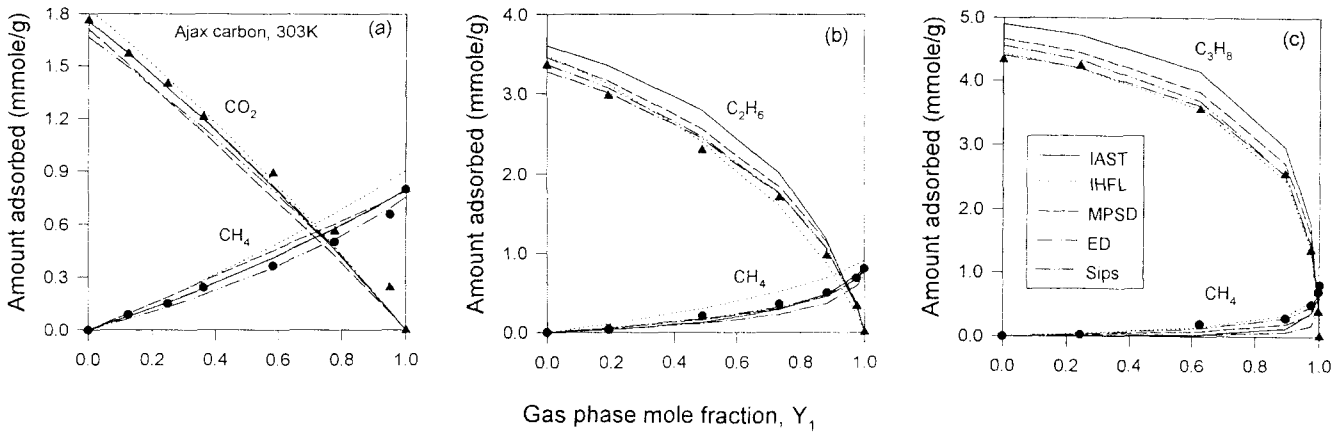

Figure 3. Prediction of binary adsorption equilibrium of (a) CH_4 (1)–CO_2 (2); (b) CH_4 (1)–C_2H_6 (2); and (c) CH_4 (1)–C_3H_8 (2) on Ajax-activated carbon at 303 K and 66. 7 KPa.

tem the IHFL is seen to be the best model for fitting the experimental data. From a comparison of the amounts of methane adsorbed on the Ajax and Nuxit-al-activated carbons with the values for NSK25 carbon in all different systems, it is clear that this chemically activated carbon (NSK25) has more capacity per mass basis for methane. This is due to the smaller mean pore size as well as the narrower pore-size distribution, as shown in Figure 2.

The adsorption behavior of the three binary systems on NSK100 carbon is shown in Figure 7. The first observation is the increase in the amount of methane adsorbed compared to the same system using commercial activated carbons (about twice) and even NSK25 carbon. Apart from the reason mentioned in the NSK25 case, higher adsorption of methane in NSK100 carbon is due to the higher micropore volume compared to that of NSK25 (see Figure 2). The second observation is the presence of a small hump in the adsorption curve of methane in both the methane–CO_2 and methane–propane systems. This nonideal behavior of this carbon is explained later. Again, most of the models do not describe well the equilibrium data of these binary systems. In particular, the predictions of methane adsorption deviate substantially from the experimental data. The poor predictions of all models for NSK data could be due to the complex structure of these chemically activated carbons, which none of the present models are capable of describing. For the methane–ethane system the only model that can predict the experimental data of both adsorbates fairly well is the IHFL model. In the methane–propane system, all the models overpredict the propane adsorption and underpredict the methane adsorption.

Figure 8 shows the binary equilibrium data on NSK500 carbon. The figure shows that the amount of methane adsorbed in this carbon is also about twice that of those of com-

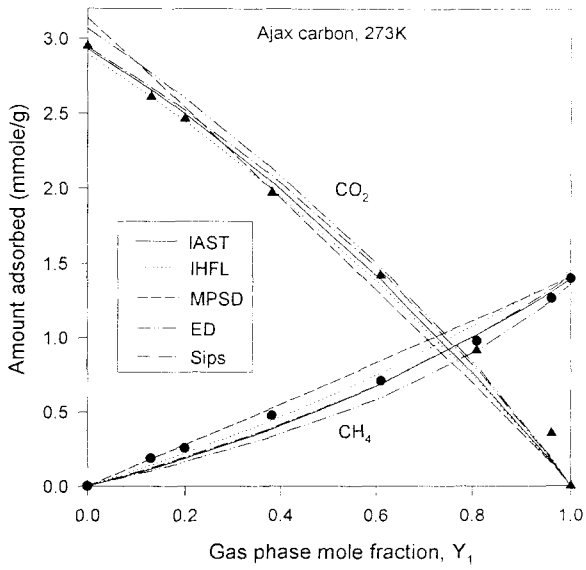

Figure 4. Prediction of binary adsorption equilibrium of CH_4 (1)–CO_2 (2) on Ajax-activated carbon at 273 K and 66.7 kPa.

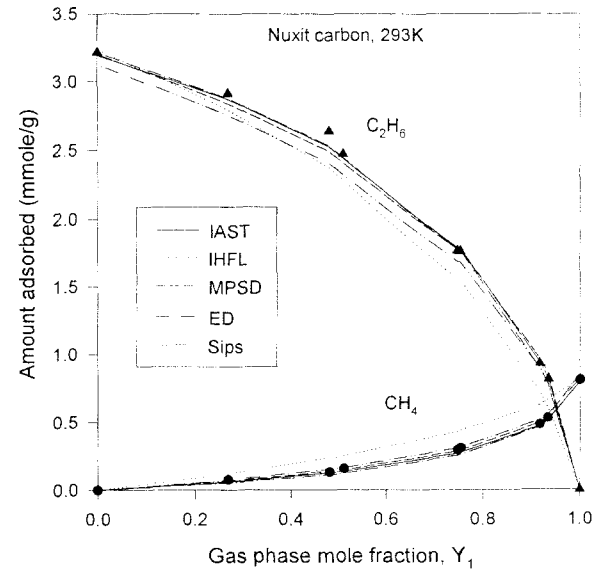

Figure 5. Prediction of binary adsorption equilibrium of CH_4 (1)–C_2H_6 (2) on Nuxit-al-activated carbon at 293 K and 100 kPa.

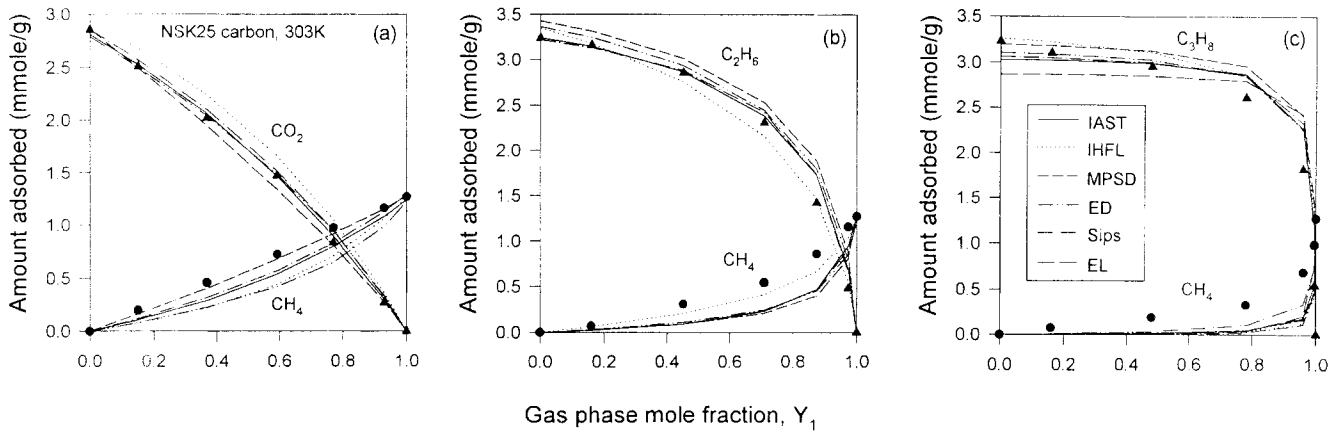

Figure 6. Prediction of binary adsorption equilibrium of (a) CH_4 (1)–CO_2 (2); (b) CH_4 (1)–C_2H_6 (2); and (c) CH_4 (1)–C_3H_8 (2) on NSK 25 activated carbon at 303 K and 66.7 kPa.

mercial ACs. This is because of the large volume of the micropores developed under the effects of KOH during the carbonization process. The predictions of the different models in the figure show that all the models underpredict the adsorption behavior of the light component (CH_4), but the quality of fitting is much better in the case of the IHFL model. For ethane adsorption all the models, except IHFL, slightly overpredict the amount of this component adsorbed.

One reason for the higher adsorption of methane in NSK carbons as compared to those predicted by different models seems to be the large amount of functional groups on the carbon surfaces. As stated before, a considerable number of surface functional groups, such as R–COOH, R–OCO, R–OH, and R = 0, were found by Otowa et al. (1996) on the carbons prepared by the KOH activation technique. The effect of these functional groups plus the imperfections, such as holes in the structure of carbon, on the adsorption behavior are not considered explicitly in any of these models, therefore their predictions deviate greatly from the experimental results. The IHFL model, which takes into account some degrees of heterogeneity in the carbon by the pattern of isosteric heat, is seen to predict the adsorption of both light and heavy species better than the other models.

The methane–propane system in Figure 8c exhibits a similar hump in the adsorption behavior of methane at high concentration as observed in the NSK100 carbon. To clearly show the differences in the binary adsorption of methane and propane in the NSK carbon series, the experimental data are plotted in Figure 9. In the figure the graphs represent the best lines that passed through the experimental data. The change in the amount of methane and propane by increasing the ratio of chemical to nutshell can be seen in the figure. The NSK25 carbon has more affinity toward propane, as its adsorbed concentration exhibits a very small change when the mole fraction of methane in the gas phase increases. A lower micropore size range in this carbon produces stronger adsorption forces for propane molecules. The nonideal behavior of the methane adsorption on the NSK100 and NSK500 carbons (the presence of the humps) can be explained as follows. As discussed earlier, NSK carbons accommodate a large portion of micropores in their structures. Most of these pores, which are in the size range of the molecular dimension of the hydrocarbon species used in the present study, induced some extra potential energy during the adsorption process. The adsorption of heavier hydrocarbon molecules such as propane could result in the evolution of a large quantity of heat, which

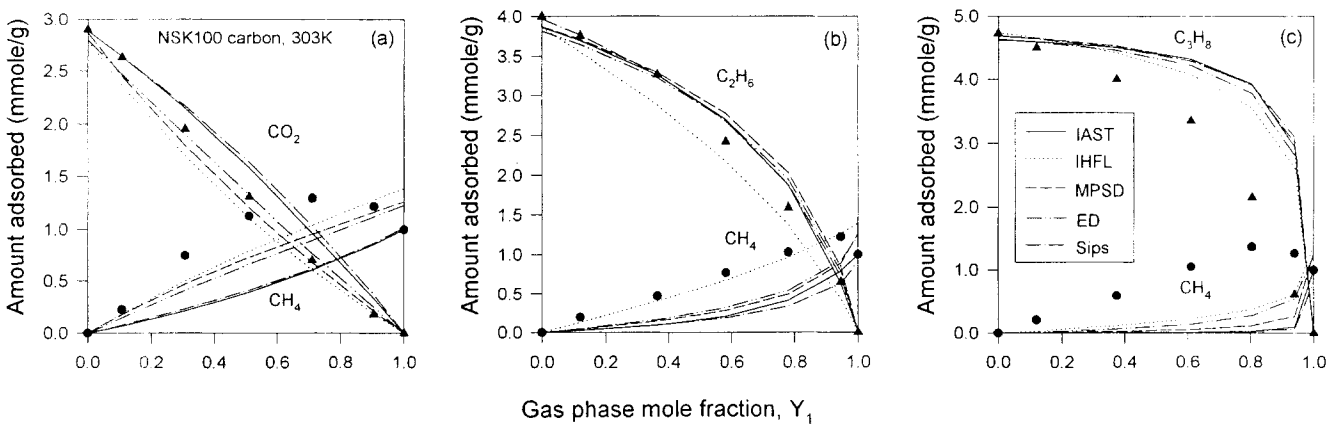

Figure 7. Prediction of binary adsorption equilibrium of (a) CH_4 (1)–CO_2 (2); (b) CH_4 (1)–C_2H_6 (2); and (c) CH_4 (1)–C_3H_8 (2) on NSK100-activated carbon at 303 K and 66.7 kPa.

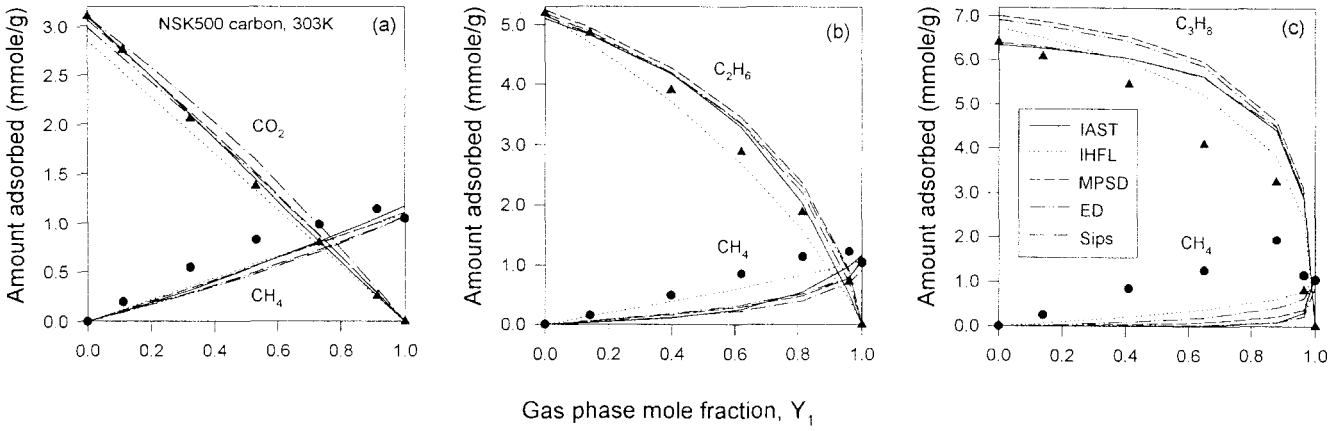

Figure 8. Prediction of binary adsorption equilibrium of (a) CH_4 (1)–CO_2 (2); (b) CH_4 (1)–C_2H_6 (2); and (c) CH_4 (1)–C_3H_8 (2) on NSK500-activated carbon at 303 K and 66.7 kPa.

locally causes some swelling in the particle and a small increase in the pore volume. It should be mentioned that in the binary adsorption of methane and propane a temperature increase of more than 10 K in the adsorbed phase is observed for NSK carbons. By increasing the size of those pores that were originally slightly larger than one propane molecule, there will be room for another layer of smaller methane molecules. These methane molecules, due to the pore wall effect and also the effect of neighboring propane molecules, rearrange in such a way that they are more compactly arranged than when they are adsorbed in the pure state. Therefore, a small increase in the adsorbed amount of methane in the binary system compared to that of the pure methane can be seen for these two NSK carbons. In the case of NSK25, most of the micropores are in the smaller range than that of the other two carbons, and even by increasing the pore widths due to the heat effect, those pores are not large enough to accommodate one layer of methane along with the propane molecules.

To give a clear picture of the phenomena observed in Figure 9, we have presented a model for the adsorption of methane in the pure as well as in the binary states. The model is given in Figure 10. As previously stated, due to their presence at the supercritical state (see Figure 10a), methane molecules may not be so compact in their adsorbed form during the pure-component adsorption. On the other hand, in the presence of propane molecules and inside the confined pores these molecules become closer to each other, and the net result can be a greater increase in the adsorption capacity for methane in the binary state than in the pure state (Figure 10b).

To compare the affinity of the activated carbons for methane adsorption in the presence of other species, the experimental results of the methane mole fraction in the gas phase vs. those in the adsorbed phase (known as the *X-Y* diagram) are plotted in Figure 11. The information present in this figure showed that NSK carbons have more affinity for methane molecules in all three binary systems than the commercial Ajax-activated carbon. This is because of the PSD and the presence of the functional groups in this series of

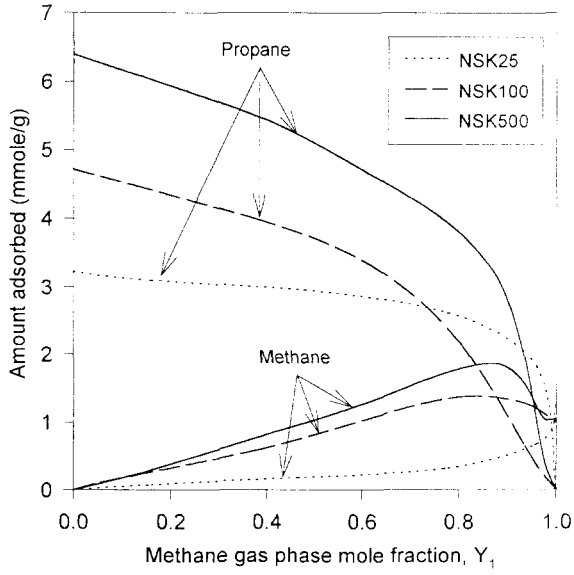

Figure 9. Experimental binary adsorption data of CH_4 (1)–C_3H_8 (2) on NSK-activated carbons at 303 K and 66.7 kPa.

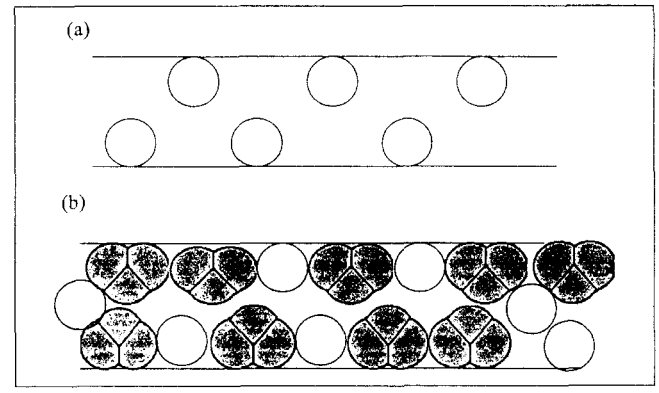

Figure 10. Models for (a) adsorption of pure methane, and (b) coadsorption of methane–propane on slit-shaped pores of activated carbons.

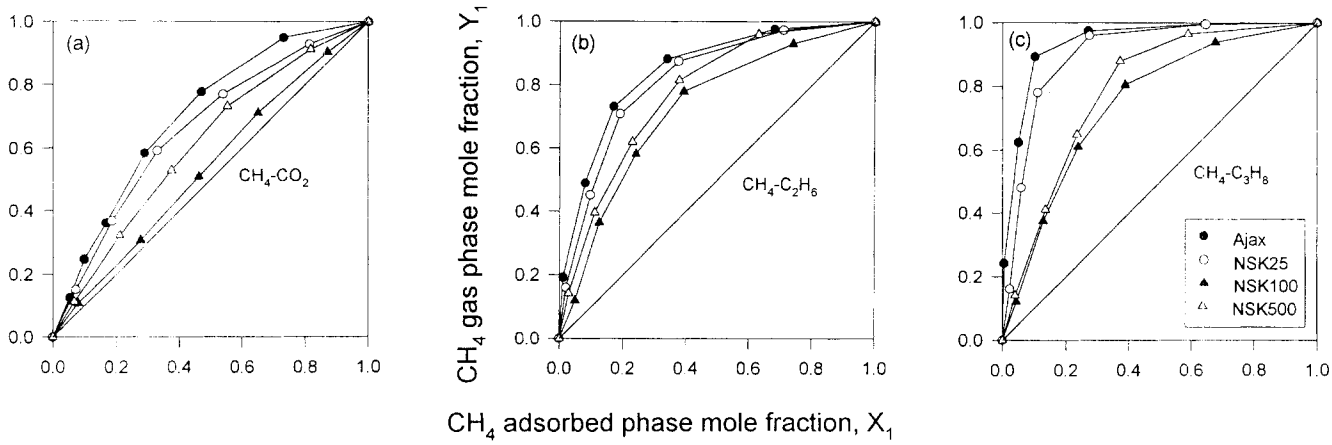

Figure 11. *X-Y* diagram for (a) CH_4 (1)–CO_2 (2); (b) CH_4 (1)–C_2H_6 (2); and (c) CH_4 (1)–C_3H_8 (2) on Ajax- and NSK-activated carbons at 303 K and 66.7 kPa.

carbons as discussed earlier. The order of methane adsorption affinity in different carbons is NSK100 > NSK500 > NSK25 > Ajax.

Finally, the qualitative comparison of all six models investigated in the present study are summarized in Table 17. The models are ranked in the table in three categories based on their goodness of fit. Most of the models fit the experimental data of the physically activated carbons well, but only the IHFL model can better predict the data in the nutshell chemically activated carbons.

Conclusions

Binary adsorption of methane with two heavier hydrocarbons (ethane and propane) and CO_2 are studied in a series of chemically activated carbons with different pore structures. It was found that the pore structure has a significant influence on the binary adsorption behavior. Two commercial ACs are also studied for comparison purposes. The presence of heavy hydrocarbons and CO_2, which are considered to be impurities in the NG, not only reduce the methane adsorption but in carbons activated with KOH cause a positive impact. The experimental data have been predicted with six different multicomponent adsorption models. While all the models work reasonably well for the commercial ACs, only the IHFL model, which takes into account the heterogeneity of carbons through the adsorbate–adsorbent interactions, can predict the experimental data of NSK carbons with a reasonable accuracy.

Table 17. Comparison of the Models in Terms of Their Goodness of Fit*

		Models					
Carbons	System	IAST	IHFL	MPSD	ED	Sips	EL
Nuxit-al	CH_4–C_2H_6	G	G	G	G	G	G
Ajax	CH_4–CO_2	G	A	A	G	G	G
	CH_4–C_2H_6	B	G	G	G	G	G
	CH_4–C_3H_8	B	G	G	G	A	A
NSK25	CH_4–CO_2	A	B	G	B	A	A
	CH_4–C_2H_6	A	G	A	A	A	A
	CH_4–C_3H_8	B	B	B	B	B	B
NSK100	CH_4–CO_2	B	B	B	B	B	B
	CH_4–C_2H_6	B	G	B	B	B	B
	CH_4–C_3H_8	B	B	B	B	B	B
NSK500	CH_4–CO_2	A	A	B	B	B	B
	CH_4–C_2H_6	B	A	B	B	B	B
	CH_4–C_3H_8	B	B	B	B	B	B

*G: good; A: acceptable; B: bad.

Acknowledgment

The authors wish to thank the Austrailian Research Council for its support. The first author is grateful to the Ministry of Culture and Higher Education of Iran and the Department of Chemical Engineering, University of Queensland for the scholarship grant.

Notation

b = adsorption affinity, kPa^{-1}
b_0 = adsorption affinity at zero energy level, kPa^{-1}
C_μ = adsorbed phase concentration, mmol/g
$C_{\mu s}$ = maximum adsorbed phase concentration, mmol/g
M = molecular weight, g/mol
n = parameter in the Sips equation
P = adsorption pressure, kPa
q = gamma distribution parameter, $Å^{-1}$
R = gas constant
T = temperature, K
x = mole fraction in the adsorbed phase
x_{min} = the minimum reduced pore half-width
y = mole fraction in the gas phase
z = distance between adsorbate and pore central plane, Å

Greek letters

β = the affinity parameter $kPa^{-1}\sqrt{K \times g/mol}$
δ = thermal expansion coefficient, K^{-1}
ϵ = particle porosity
$\varphi(z,r)$ = pore potentials at distance z in pore with radius r, J/mol
η = parameter defined by Eq. 2
γ = distribution parameter
Γ = gamma function

Literature Cited

Ahmadpour, A., and D. D. Do, "Characterization of Modified Activated Carbons: Equilibria and Dynamics Studies," *Carbon*, **33**, 1393 (1995).

Ahmadpour, A., and D. D. Do, "The Preparation of Active Carbons from Coal by Chemical and Physical Activation," *Carbon*, **34**, 471 (1996).

Ahmadpour, A., and D. D. Do, "The Preparation of Activated Carbon from Macadamia Nutshell by Chemical Activation," *Carbon*, **35**, 1723 (1997).

Do, D. D., and H. D. Do, "A New Adsorption Isotherm for Heterogeneous Adsorbent Based on the Isosteric Heat as a Function of Loading," *Chem. Eng. Sci.*, **52**, 297 (1997).

Kapoor, A., and R. T. Yang, "Correlation of Equilibrium Adsorption Data of Condensible Vapours on Porous Adsorbents," *Gas Sep. Purif.*, **3**, 187 (1989).

Myers, A. L., and J. Prausnitz, "Thermodynamics of Mixed Gas Adsorption," *AIChE J.*, **11**, 121 (1965).

Nguyen, C., A. Ahmadpour, and D. D. Do, "Effect of Gasifying Agents on the Characterization of Nutshell-derived Activated Carbon," *Adsorption Sci. Tech.*, **12**, 247 (1995).

O'Brien, J. A., and A. L. Myers, "Physical Adsorption of Gases on Heterogeneous Surfaces—Series Expansion of Isotherms Using Central Moments of the Adsorption Energy Distribution," *J. Chem. Soc., Faraday Trans.*, **80**, 1467 (1984).

O'Brien, J. A., and A. L. Myers, "Rapid Calculations of Multicomponent Adsorption Equilibria from Pure Isotherm Data," *Ind. Eng. Chem. Process Des. Dev.*, **24**, 1188 (1985).

O'Brien, J. A., and A. L. Myers, "A Comprehensive Technique for Equilibrium Calculations in Adsorbed Mixtures: The Generalized FastIAS Method," *Ind. Eng. Chem. Res.*, **27**, 2085 (1988).

Otowa, T., Y. Nojima, and M. Itoh, *Fundamentals of Adsorption*, M. D. LeVan, ed., Kluwer, Boston, p. 709 (1996).

Rudzinski, W., K. Nieszporek, H. Moon, and H. K. Rhee, "On the Theoretical Origin and Applicability of the Potential Theory Approach to Predict Mixed-Gas Adsorption on Solid Surfaces from Single-Gas Adsorption Isotherms," *Chem. Eng. Sci.*, **50**, 2641 (1995).

Ruthven, D. M., *Principles of Adsorption and Adsorption Processes*, Wiley, New York (1984).

Sips, R., "On the Surface of a Catalyst Surface," *J. Chem. Phys.*, **16**, 490 (1948).

Steele, W. A., *The Interaction of Gases with Solid Surfaces*, Pergamon, New York (1974).

Valenzuela, D. P., and A. L. Myers, *Adsorption Equilibrium Data Handbook*, Prentice-Hall, Englewood Cliffs, NJ (1989).

Valenzuela, D. P., A. L. Myers, O. Talu, and I. Zweibel, "Adsorption of Gas Mixtures: Effect of Energetic Heterogeneity," *AIChE J.*, **34**, 397 (1988).

Wang, K., and D. D. Do, "Effects of Micropore Size Distribution on the Sorption Equilibria and Kinetics of Hydrocarbons onto Activated Carbons," Pacific Basin Workshop on Adsorption Science and Technology, Kisarazu, Japan (1997).

Wang, K., A. Ahmadpour, and D. D. Do, "Equilibria and Kinetics Characterization of Two Different Structured Nutshell-Derived Activated Carbons," *Adsorption*, **3**, 267 (1997).

Manuscript received June 16, 1997, and revision received Nov. 24, 1997.